Evaluation of the Shallow Gas Hydrate Production Based on the Radial Drilling-Heat Injection-Back Fill Method

CHEN Qiang[1), 2), 4)], WAN Yizhao[1), 2), 4)], WU Nengyou[1), 2), *], SUN Jianye[1), 2), 4)], WANG Jian[3)], LIU Changling[1), 2)], LI Yanlong[1), 2), 4)], LI Chengfeng[1), 2)], and HU Gaowei[1), 2), 4)]

1) *Key Laboratory of Gas Hydrate, Ministry of Natural Resources, Qingdao* 266071, *China*
2) *Laboratory for Marine Mineral Resources, Laoshan Laboratory, Qingdao* 266071, *China*
3) *CNPC Offshore Engineering Company Limited, Beijing* 100028, *China*
4) *Technology Innovation Center for Marine Methane Monitoring, Ministry of Natural Resources, Qingdao* 266071, *China*

Abstract It has been evidenced that shallow gas hydrate resources are abundant in deep oceans worldwide. Their geological background, occurrence, and other characteristics differ significantly from deep-seated hydrates. Because of the high risk of well construction and low production efficiency, they are difficult to be recovered by using conventional oil production methods. As a result, this paper proposes an alternative design based on a combination of radial drilling, heat injection, and backfilling methods. Multi-branch holes are used to penetrate shallow gas hydrate reservoirs to expand the depressurization area, and heat injection is utilized as a supplement to improve gas production. Geotechnical information collected from an investigation site close to the offshore production well in the South China Sea is used to assess the essential components of this plan, including well construction stability and gas production behavior. It demonstrates that the hydraulic fracturing of the 60 mbsf overburden layer can be prevented by regulating the drilling fluid densities. However, the traditional well structure is unstable, and the suction anchor is advised for better mechanical performance. The gas production rate can be significantly increased by combining hot water injection and depressurization methods. Additionally, the suitable production equipment already in use is discussed.

Key words shallow gas hydrate; trail production; radial drilling-heat injection-back fill method; experimental and numerical simulation

1 Introduction

According to different accumulation depths, there are two primary forms of gas hydrates in the marine environment: deep seated gas hydrates and shallow gas hydrates (Collett *et al.*, 2015; Boswell *et al.*, 2016). The former typically occurs as pore filling and is buried more than 100 m below the seafloor (mbsf). The bulk shallow gas hydrates are typically buried less than 60 mbsf. Different formation mechanisms determine their accumulation models: shallow gas hydrate is accumulated by deep hydrocarbon sources overflowing along the fracture or gas chimney to near the sea bottom, whereas deep seated gas hydrate is mainly formed by methane diffusion through sediments (Fig.1).

Based on the most recent geological survey findings, it has been confirmed that there are vast amounts of shallow gas hydrate resources (Luan *et al.*, 2008; Pape *et al.*, 2011; Waage *et al.*, 2019; Snyder *et al.*, 2020a). These resources have been widely discovered in areas including the eastern marginal Sea of Japan, the Gulf of Mexico, the Okhotsk Sea, and the Barents Sea. For instance, the eastern side of the Japan Sea and Hokkaido is host to more than 1700 unique geological features, including hydrate mounds and pockmarks, and numerous hydrate samples have been obtained there. Fig.2 displays a 6 m thick bulk hydrate core obtained by a piston corer at a depth of 17 m. Some main characteristics can be indicated from that: 1) bulk shape occurrence, specifically nodular, lenticular, and thick layered; 2) superficial buried depth, commonly less than 60 mbsf; 3) enormous resource potential, about 600 million cubic meters of methane in a single gas chimney.

Boswell and Collett (2006) have pointed out that the second most promising oceanic hydrate resource in the 'Gas hydrate Resource Pyramid' is the shallow hydrate, just below the sand-dominated hydrate. Therefore, it has become an international magnet for mining targets. Japan has initiated prospective studies (Matsumoto and Aoyama, 2020). In addition to the two offshore trial productions (Fujii *et al.*, 2015; Konno *et al.*, 2017; Yamamoto *et al.*, 2019), Japan launched the 'Detection and Development of Shallow Gas Hydrate Resources' project in 2013, which consists of four stages: academic research, resource investigation, resource development technology innovation, and resource production. For now, it has entered the third stage. The main tasks are listed as follows.

* Corresponding author. E-mail: wuny@ms.giec.ac.cn
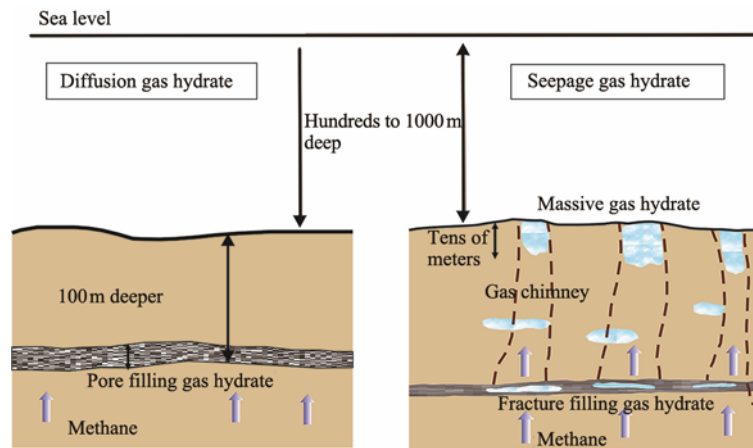
Fig.1 Sketch of the marine gas hydrate accumulation process.
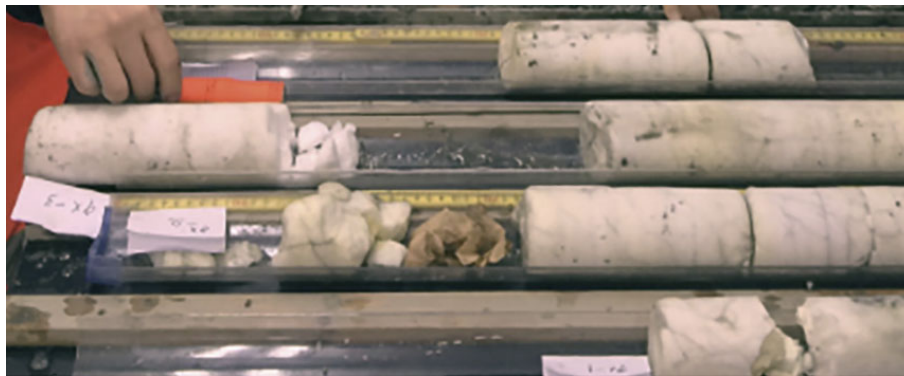
Fig.2 Methane hydrate core obtained from the eastern margin of the Japan Sea (Snyder *et al.*, 2020b).

1) Making technical schemes for the exploitation, recovery, and transportation of shallow hydrates, such as hydrate crushing and decomposition, gas collection, solid-liquid-gas three-phase control, hydrate storage, and recovery, *etc*.

2) Evaluate the feasibility of the above scheme, including whether it is suitable for the recovery and transportation of shallow surface hydrate, its recovery rate, recovery time, stability, and safety, especially the economic evaluation of long-term mining.

3) Formulate emergency plans, including emergency plans in case of mud and water production, assess the safety risks of recovery equipment in case of emergencies, reduce environmental hazards to the ocean and atmosphere, and assess the stability of mining reservoirs.

China also emphasized gas hydrate production, aiming to realize industrialized development. In 2017 and 2019, China successfully implemented two offshore trial productions, creating a record of $86.14 \times 10^4 \, \text{m}^3$ gas production in 30 days (Li *et al.*, 2018; Ye *et al.*, 2020). Shallow gas hydrate has also been found in the South China Sea. During the cruises of GMGS2-08/GMGS2-09/GMGS2-16 carried out by the China Geological Survey (CGS), core samples with shallow hydrate were obtained. The bulk hydrate occurrence is vein nodular and massive, and the buried depth range is from 8 to 30 mbsf (Liu *et al.*, 2021).

However, in the past trial productions, the depressurization method was mainly used to dissociate the pore filling hydrate at about 200 mbsf (Schicks *et al.*, 2020; Wang *et al.*, 2020; Wu *et al.*, 2020). The production equipment and scheme cannot directly apply to shallow gas hydrate. Firstly, there are no pores in the shallow bulk hydrate, which leads to low efficiency of heat and pressure transfer, and the gas production law is essentially different from pore filling hydrate reservoir. Secondly, the thinner overburdened sediment may not supply enough mechanical bearing capacity, and a large empty area would be left after the hydrate is dissociated and collected, leading to formation collapse (Kong *et al.*, 2018). Therefore, a reasonable production plan is essential for the gas hydrate development strategy.

Researchers have already put forward some schemes to produce shallow gas hydrates (Zhang and Lu, 2016; Zhou *et al.*, 2017a; Kong *et al.*, 2018; Xu *et al.*, 2018). For example, Zhou *et al.* (2017b) proposed a solid fluidization mining method. After converting the solid bulk hydrate into a fluid state through mechanical crushing, the liquid-solid multiphase material was lifted through a pipeline. The hydrate particles will be gradually gasified during the lifting process as the seawater temperature increases and the hydrostatic pressure decreases. One problem is that the physical environmental impact on the seabed is unclear.

In summary, no actual trial attempt has been carried out internationally on shallow gas hydrate due to immature production technology and environmental constraints. In

this paper, an alternative scheme is proposed for the recovery of shallow bulk hydrates using multi-branch hole depressurization technique, supplemented by thermal injection and the goaf refill process. Key aspects of this scheme are evaluated, and equipment support conditions are discussed to prove its feasibility further.

2 Well Construction and Production Procedure

The production system consists of three parts: the drilling and wellbore constructing section, the artificial lifting section, and the proppant backfilling section. The most critical function of the drilling and wellbore section is to overcome the low sediment resistance at shallow depth, providing sufficient mechanical capacity for the entire production system. Here the suction anchor is recommended, and detailed analysis is shown below. Meanwhile, the hydrate dissociation surfaces should be increased as much as possible, which is helpful in gas production. So, multiple horizontal sidetracking modules are necessary (Li *et al.*, 2019b). It can penetrate and divide the bulk hydrate layer with micro-fracture. Studies have shown that heat excitation is more efficient than depressurization for the bulk hydrate dissociation (Chen *et al.*, 2020). So, in this design, the artificial lifting section contains an electric submersible pump (ESP) and a thermal-fluid injection pump (TIP). ESP is used to depressurize mining, and TIP is used to heat injection. As we will discuss below, the alternative use of these two pumps can achieve good gas production results. When bulk hydrate is dissociated and pumped out, empty goaf will be left in the layer. Therefore, the last but not least section is proppant backfilling by the mortar pump (MP). Packing the goaf with unique materials, such as the resin-coated sand, the reservoir will be reinforced as mining continues, guaranteeing the absolute production security. The well construction system is shown in Fig.3.
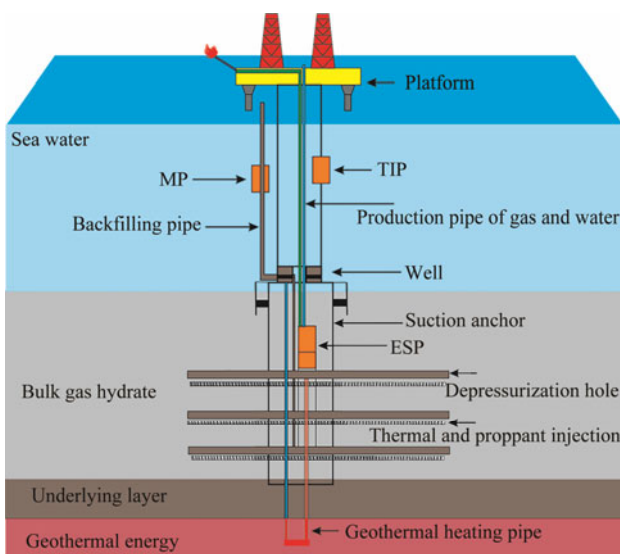
Well construction and production procedures are described as follows:

1) Use jetting conductor or suction anchor to create a large diameter vertical wellbore. A bunch of depressurization holes and agent injection holes are drilled by a horizontal sidetracking module at different depths on both sides. At the current level of drilling technology, the maximum length of these branch holes is about 100 m in the clayed silt sediment.

2) After the drilling process, the ESP/TIP/MP are installed at different positions. Three kinds of pumps can be switched manually to fulfill the tasks of pressure drop, thermal-fluid inject, and propane fill. A three-phase separator of gas-water-sand is placed on the production line.

3) Start the ESP to reduce the pressure around the branch holes during production. Gas will be collected through the pipeline after the hydrate decomposition. Real-time monitoring of gas and water production is necessary to estimate the deficit of the hydrate reservoir. Branch holes are opened from bottom to top in sequence in order to mine the lower part first and fill the goaf soon, which is beneficial to the reservoir security.

4) When the gas production rate has dramatically decreased, the thermal-fluid must be pumped into the layer and soaked for a certain time to stimulate more hydrate dissociation. Hot water would be a good choice, particularly at the production sites with good geothermal resources in deeper formation.

5) Gas production continues with ESP pumping and TIP soaking alternatively until the formation stability is close to failure. Then proppant injection procedure starts. Materials like resin-coated sands are pumped into the goaf by MP and fill the empty zone to recover the bearing capacity of soils. After that, open the upper branch holes and repeat the above steps until the production work finishes. The recovered gas and gas-saturated liquid are transported to the deck for further treatment.

3 Scheme Feasibility Evaluation

3.1 Soil Parameters

Multiple drilling programs conducted by the CGS have proved the widespread distribution of gas hydrates on the northern slope of the South China Sea, including deep-seated gas hydrates and shallow gas hydrates. In this paper, we take the investigation data at one geotechnical site to evaluate our proposed design. The site is near the offshore production well, with a water-depth of about 1000 m. The sediment deposited on the continental slope is dominated by hemipelagic fine-grained sediments (Li *et al.*, 2012). Soil properties are obtained by *in-situ* piezocone penetration test (PCPT) and laboratory testing, as shown in Table 1.

3.2 Well Construction Stability Analysis

The overburden strata of shallow hydrates are commonly composed of newly deposited and unconsolidated sediments, such as clay, sand, or mudstone. So, there would be a high possibility of insufficient wellbore stability. For dril-

Fig.3 The sketch diagram of the bulk hydrate production system based on the radial drilling-heat injection-back fill method.

Table 1 Soil design parameters and effective soil strength parameters

Depth (mbsf)	Undisturbed shear strength (kPa)		Remoulded shear strength (kPa)		ε_{50} (%)	Effective friction angle (Φ')	Effective cohesion (c') (kPa)	Young's modulus (E_0) (Mpa)
	Low estimate	High estimate	Low estimate	High estimate				
0.0	1.0	3.0	0.3	0.8	2.0	19	0.8	5
5.6	17.0	160.0	4.3	45.7	2.0	34	12.0	105
11.9	140.0	205.0	26.0	45.0	2.0	28	55.0	155
18.5	160.0	225.0	30.0	54.0	2.0	35	9.0	180
28.9	160.0	240.0	24.0	42.0	0.8	35	7.0	225
38.5	140.0	250.0	24.0	41.7	2.0	34	8.0	270
56.3	170.0	288.0	32.0	48.0	2.0	26	80.0	370
63.6	150.0	210.0	37.5	52.5	3.0	19	0.8	395

Note: ε_{50}, vertical strain at half of the maximum deviator stress.

ling in the shallow reservoir, the construction is mainly composed of a 914 mm diameter conductor with jetting string and a 340 mm diameter casing. So, we first evaluate the stability parameters of this well construction. The buoyant weight is set to 529 kN, and the jetted depth is set to 60 m for calculation.

The immediate axial capacity of a jetted conductor is equivalent to the load required to penetrate the formation during its installation or immediately after its installation. During installation, the jetting process removes the soil beneath the conductor's tip, lowering the lateral soil pressure acting on the conductor and reducing the soil resistance, leading to more significant uncertainty in conductor shaft friction.

Soil parameters required for the jetted conductor analysis include undisturbed undrained shear strength, remoulded undrained shear strength, and ε_{50} (listed in Table 1). The immediate axial capacity of a jetted conductor can be estimated according to the following relationship:

$$Q_1 = Q_s = fA , \qquad (1)$$

where, Q_1 is immediate axial capacity prior to reciprocation, Q_s is compressive/tensile capacity available from external friction acting on the conductor, f is unit skin friction acting on the outer surface of the conductor, A is the external surface area of the conductor.

The unit skin friction, varying with depth, is primarily the function of the soil shear strength for clay or the effective vertical stress and internal friction angle for sand. The immediate axial capacity of a jetted conductor is equivalent to the load required to penetrate the formation during or immediately after its installation. Fig.4 depicts the immediate axial capacity of the conductor at the setting depths of 40 m, 50 m, and 60 m and the range of the WOB during the conductor installation. It indicates that the immediate axial conductor capacity could vary between 75% and 100% of the maximum available weight-on-bit (WOB) during installation.
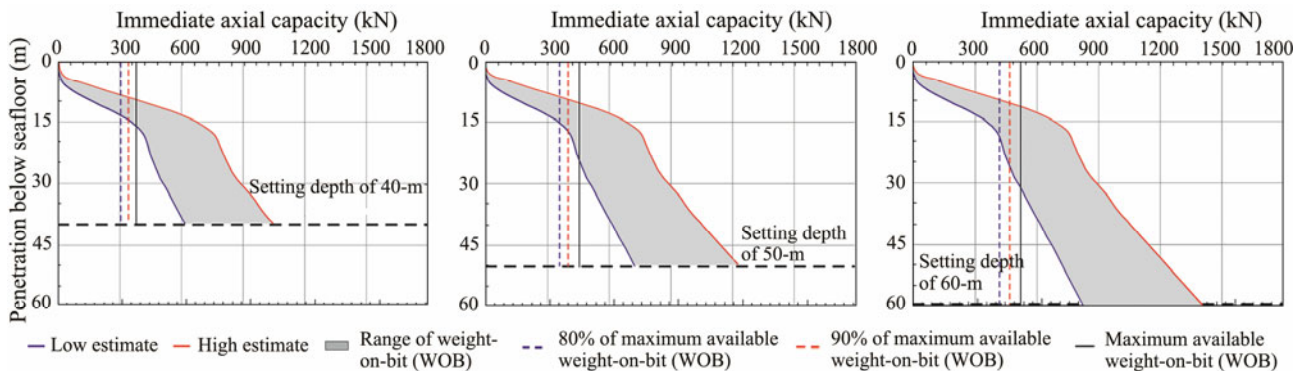
Fig.4 Estimated immediate axial capacity at different depth.

The analysis shows that soil conditions can be determined, and the final applied WOB is the most influential parameter affecting the conductor performance. Although the installation of conventional jet conductors can be done with the correct WOB, there is a considerable risk during mining. As the bulk hydrate is dissociated and pumped out, the conductor bearing capacity decreases significantly. Therefore, it is recommended to use a sizeable implantable wellbore structure such as suction anchor (Fig.5). The suction anchor conduit is composed of a large cylinder and some internal constructions, with a diameter of 4–8 m and a leng-

th of 12–15 m. A single conduit or multiple conduits can be installed inside.

The friction calculation formula of single barrel suction anchor is as follows:

$$Q_t = Q_0 + W_{\text{outerwall}}(\Delta\alpha_t, Su_{\text{ave}}) + W_{\text{innerwall}}(\Delta\alpha_t, Su_{\text{ave}}) + W_{\text{end}}(Su) , \qquad (2)$$

where Q_t is time-dependent bearing capacity, Q_0 is instantaneous frictional resistance, W is resistance, $\Delta\alpha_t$ is soil strength restoration factor, Su_{ave} is the average shear streng-

th of soil, *Su* is end soil shear strength.
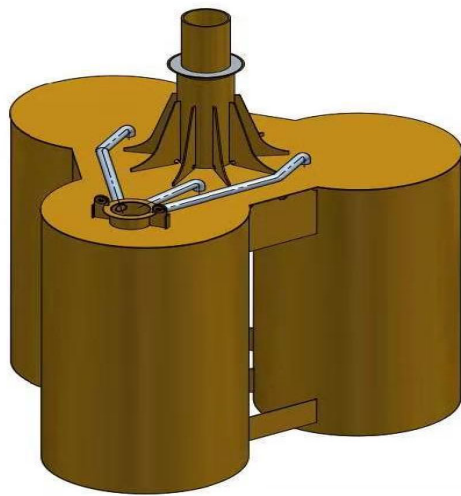
Fig.5 Ssketch of the suction anchor with multi conduits.

When the suction anchor is placed to the predetermined depth, the resistance varies based on various factors such as external wall shear friction and internal wall shear friction. Due to the large outer diameter, the suction anchor conduit can provide a huge load capacity. Even if the buried depth of hydrate is further reduced, for example, only 10 mbsf, the multi conduit suction anchor can provide enough load capacity to stabilize the well construction.

3.3 Hydraulic Fracture Assessment

In this study, the hydraulic fracture pressure was predicted based on the shear failure model for cohesive soils developed by Aldridge and Haland (Aldridge and Haland, 1991). The model considers an undrained plastic failure mechanism at the borehole wall. Accordingly, the formation breakdown is assumed to occur when the maximum deviator stress exceeds twice the undrained shear strength of the soil. Based on this approach, the excess fracture pressure at a specific depth may be taken as the lowest values given by the following equations:

$$\Delta\Psi_f = (2K_0 - 1)\sigma'_{vo} + 2S_u, \tag{3}$$

where $\Delta\Psi_f$ is excess fracture pressure, S_u is undrained shear strength, σ'_{vo} is *in-situ* effective vertical stress, K_0 is coefficient of lateral earth pressure at rest, ranging from 0.45 to 1.6 in this calculation.

According to cavity expansion theory, the yield model for cohesionless soils considers the stress in the soil around an unsupported borehole. The definition of soil failure in the yield model is the initiation of plastic deformation at the borehole wall. The estimation of excess fracture pressure is related to the soil parameters of the *in-situ* effective stresses and the angles of internal friction. The total hydraulic fracture pressure is subsequently obtained from the equation below:

$$\Psi_f = \Delta\Psi_f + u_0, \tag{4}$$

where u_0 is pore fluid pressure at a given depth of the formation.

The predicted total hydraulic fracture pressure is shown in Fig.6, together with the estimated pressures exerted at the borehole wall by drilling fluid or grout with densities of 9, 10, 11, 12, and 13 pounds per gallon (ppg). The results indicate that drilling fluid or grout with these densities may not cause potential fracture of the soils in the top zone of 60 mbsf.
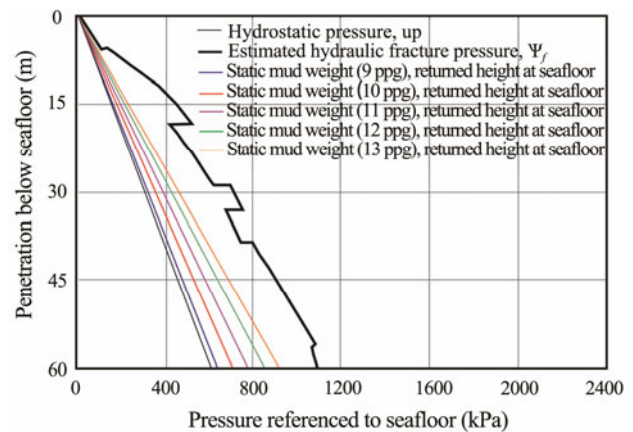
Fig.6 Hydraulic fracture pressures.

3.4 Estimation of Gas Production Behavior

According to the production scheme proposed in this study, the conceptual model, shown in Fig.7, is established with the geological parameters of the northern part of the South China Sea. The radial dimension of the model is 150 m, and the total thickness is 220 m, including 80 m of hydrate layer, 60 m of overburden layer, 30 m of underlying layer, and 50 m of branch hole.
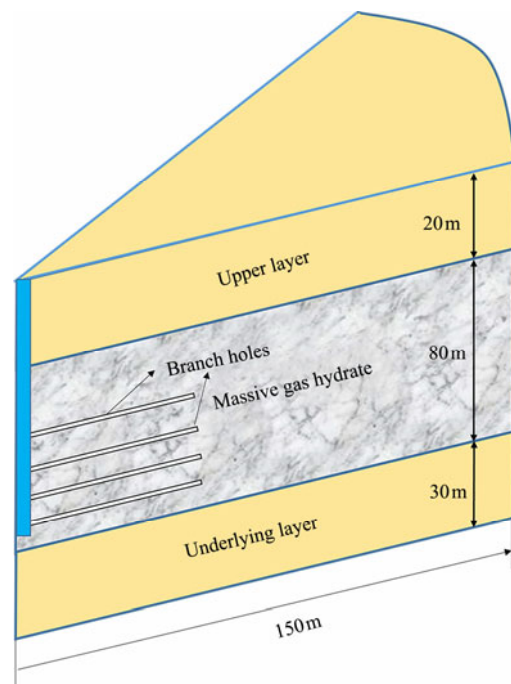
Fig.7 Conceptual model for the massive gas hydrate production.

It should be noted that the bulk gas hydrate layer is composed of pure hydrate with no sediments, and the hydrate is not porous media. Mass and heat transfer control equations are different between bulk hydrates and pore filling hydrates. Thus, the numerical simulator commonly used for the pore-filling hydrate, based on the flow theory in porous media, is inapplicable. However, the bulk hydrate can be approximately considered as pseudo-porous media with the following settings:

1) The porosity (φ) of the bulk hydrate layer is infinitely close to 1, which indicates that there is almost no skeleton and almost all the domain is pore space. Ideally, the porosity should be set to one. However, we set $\varphi = 0.98$ because of the requirement of numerical stability.

2) The hydrate saturation is set to 1, meaning that the pore space is filled with hydrates.

3) The intrinsic permeability of the hydrate layer is relatively tiny before dissociation, but it is pretty large after dissociation. When all the pore space is filled with hydrate, the pseudo-porous media is almost impermeable. However, after the hydrate is dissociated, the fluid flow in the pseudo-porous media is free because $\varphi = 1$.

TOUGH+HYDRATE (Moridis, 2014) is a famous gas hydrate numerical simulation code. The mod is used to simulate the production process based on the above settings. The parameters used in this paper are listed in Table 2. More details of the numerical model can be found in the paper by Wan *et al.* (2022).

Table 2 Main conditions and properties of the model

Parameter	Value	Parameter	Value
Thickness of bulk hydrate layer (m)	80	Porosity of overburden (%)	42
Thickness of the overburden (m)	60	Porosity of underburden (%)	38
Thickness of the underlying layer (m)	30	Porosity of massive hydrate layer (%)	98
Radius of the domain (m)	150	Wet thermal conductivity ($\mathrm{W\,m^{-1}\,K^{-1}}$)	3.1
Permeability of the overburden and underburden ($\mathrm{m^2}$)	$k_r = k_z = 1.0 \times 10^{-14}$	Dry thermal conductivity ($\mathrm{W\,m^{-1}\,K^{-1}}$)	1
Initial of permeability of the hydrate layer ($\mathrm{m^2}$)	$k_r = k_z = 1.0 \times 10^{-18}$	Water salinity (%)	3.05
Permeability of the hydrate layer after dissociation ($\mathrm{m^2}$)	$k_r = k_z = 1.0 \times 10^{-8}$	Pressure of the upper boundary (MPa)	10.91
Permeability of the branch hole ($\mathrm{m^2}$)	$k_r = k_z = 1.0 \times 10^{-8}$	Temperature of the bottom of the hydrate layer (°C)	13.69
Geothermal gradient (°C km^{-1})	50	S_{irA}	0.5
Grain specific heat ($\mathrm{J\,kg^{-1}\,°C^{-1}}$)	1000	S_{irG}	0.05
Compressibility (Pa^{-1})	1.00×10^{-8}	n_G	3
Bottom hole pressure (MPa)	4	n	5
Relative permeability model	$K_{rA} = (S_A^*)^n,$ $K_{rG} = (S_G^*)^n,$ $S_A^* = (S_A - S_{irA})/(1 - S_{irA})$ $S_G^* = (S_G - S_{irG})/(1 - S_{irA})$	Capillary pressure model	$P_{cap} = -P_0[(S^*)^{-1/\lambda} - 1]^{-1/\lambda},$ $S^* = (S_A - S_{irA})/(S_{mxA} - S_{irA})$

During the productivity simulation, the hot water injection stewing process is added as a supplementary to depressurization to enhance the decomposition effect of hydrates. Fig.8 shows the time-varying curves of gas production rates in the three stages, and Fig.9 shows the pressure and hydrate saturation fields around the branch holes.
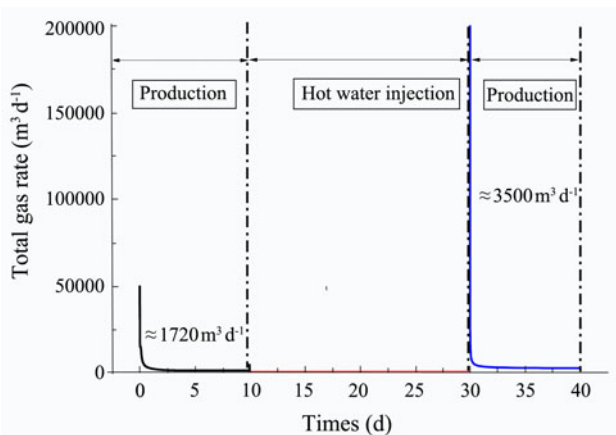
Fig.8 Time-varying curves of gas production rates in the three stages.

It can be seen that the gas production rate by depressurization in the first stage is significantly high, with an average of about $1720\,\mathrm{m^3\,d^{-1}}$ in 10 d, mainly because multi-branch holes increase the discharge area and the hydrate decomposition range is enormous. After that, hot seawater was injected and stewed for 20 d in the second stage. Then the well is opened for depressurization production again. Due to the hydrate dissociation caused by hot seawater, the gas production rate in the beginning of the third stage is very high, and the average gas production rate in 10 d of the third stage is $3500\,\mathrm{m^3\,d^{-1}}$.

3.5 Goaf Backfilling Evaluation

One of the most significant risks during the bulk hydrate production is goafs appeared after hydrate dissociation. Without the support of the solid sediment skeleton, the upper layer is prone to subsidence and collapse. In order to avoid this situation, it is necessary to backfill the goaf to recover the formation bearing capacity after a period of production.

The following equation can be used to calculate the volume of goaf:

$$V_d = \pi r_d^2 h_p, \tag{5}$$

where V_d is the goaf volume, r_d is the radius of the goaf, h_p is the thickness of the goaf.
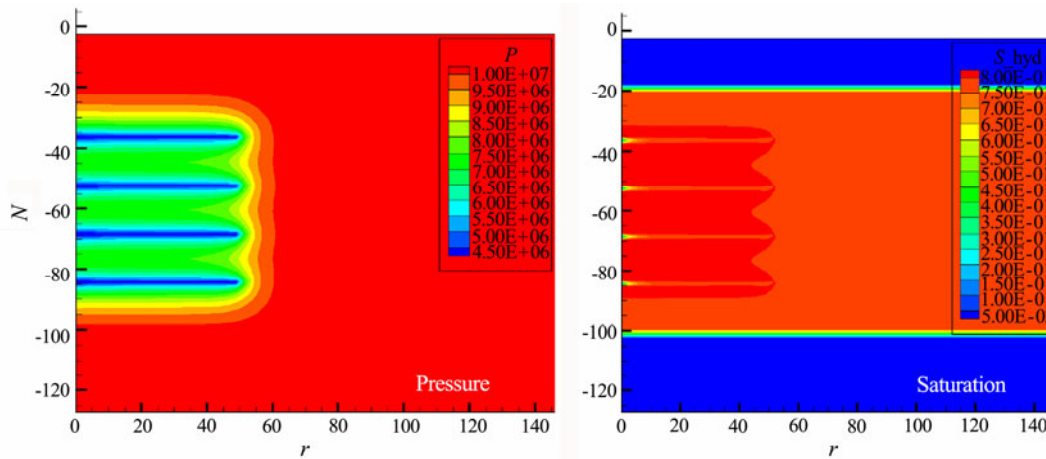
Fig.9 Pressure field and hydrate saturation field during production.

Sand particles must be filled in goaf from bottom to top, assuming the proppant as uniform spherical particles, as shown in Fig.10.
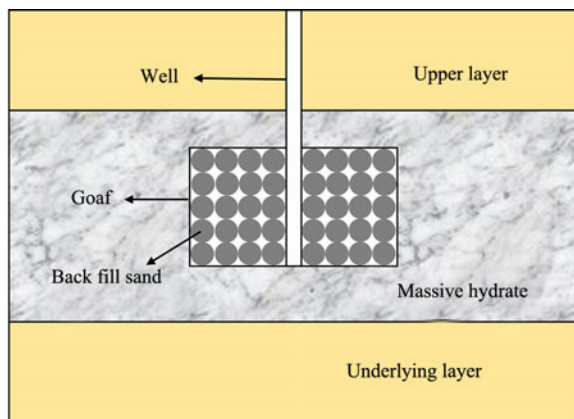
Fig.10 Sketch diagram of the hydrate dissociation area around the wellbore.

According to the random packing theory of spherical particles, the porosity of random loose packing of equal diameter spherical particles is about 40% (Allen, 1965). So, the volume of proppant used for filling is:

$$V_s = (1 - 0.4)V_d , \tag{6}$$

where V_s represents the volume of injection proppant, V_d represents the goaf volume of hydrate.

one m³ gas hydrate can produce about 160 m³ of methane gas in standard state. The dissociation gas is recovered except for a small part dissolved into water. The volume of hydrate goaf can be calculated from the gas production rate and production time, and then the volume of proppant required for filling can be calculated by Eq. (7).

$$V_s = 0.6V_d = \frac{0.6 q_g t_d}{160} = \frac{q_g t_d}{266.67} , \tag{7}$$

where q_g is the average gas production rate, t_d is produc-

tion time.

4 Support Conditions of Existing Technical Equipment

In recent years, for the sake of efficient and safe exploitation of natural gas hydrates, some innovative mining ideas have been put forward, some of which have been verified by the reliable numerical simulation (Li *et al.*, 2011; Rahim *et al.*, 2015; Feng *et al.*, 2019; Li *et al.*, 2019a). However, most of them are still in the theoretical stage and have no actual engineering construction equipment support. In order to further demonstrate the operability of this scheme, we listed some oil and gas development equipment that can realize the key steps of this production scheme.

4.1 Radial Drilling Technique

The radial drilling combines the technique of conventional horizontal well and coiled tubing. It is the extension and widening of the horizontal well technique. Drilling and injection tools are the two main modules in this technique, as shown in Figs.11 and 12, respectively. The drilling tools mainly include downhole tool combination, radial shaft, injection head, and milling bit.

The injection tool is used to make branch holes. The solid-free drilling fluid is pressurized and transmitted down to wellbore through the coiled tubing. Then the fluid sprays through the drill bit, and the high-pressure potential energy is converted into kinetic energy to generate a high-speed impulse, forming the horizontal branch hole with a radius of $3.8-7.6$ cm. Special guide shoes are used to complete the processes of deflection, orientation, and complex wellbore control. The nozzle and high-pressure hose are designed to cooperate with the coiled tubing to ensure the straightness of the wellbore. Radial drilling can be carried out in the same formation or different layers of a single well.

4.2 Goaf Filling Material

An excellent proppant is a new type of resin-coated sand
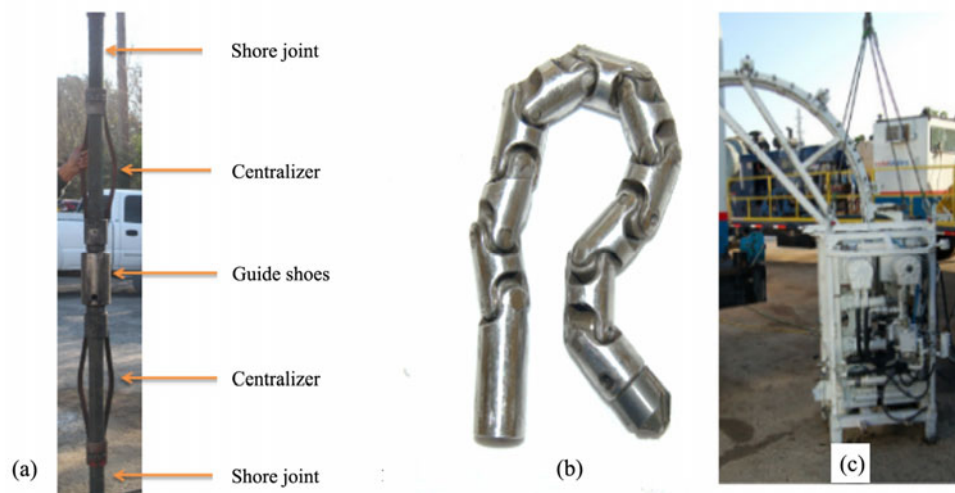
Fig.11 Drilling tools for radial horizontal wells. (a), downhole tool combination; (b), radial shaft; (c), injection head.

Fig.12 Injection tools for radial horizontal well. (a), high-pressure hose; (b), the connection between hose and coiled tubing; (c), injection bit; (d), pressure injection.

that can rapidly solidify at ultra-low temperatures. Agent A and B are created by coating the surface of the quartz sand with the ultra-low temperature fast curing resin cementation and the layer isolation agent, respectively (Fig.13). When mixed and dried, the material shows non-adhesion and good fluidity. During the *in-situ* goaf filling procedure, the resin-coated sand is carried by seawater into the target layer, where it rapidly consolidates under the low temperature of the formation, forming an artificial solid skeleton with high strength and permeability.

The main technical parameters of this resin-coated sand are listed as follows: the consolidation temperature is 20–350℃; the curing time is adjustable from 6 to 24h; the com- pressive strength is more extensive than 10 MPa; the liquid permeability is larger than $4\,\mu m^2$. The 24-h particle conso- lidation strength at 20℃ is more than 10 MPa. It can be seen that the proppant can rapidly consolidate at low tem- perature, which reduces the well occupation time and im- proves the production efficiency.

5 Conclusions

Although China, Japan and other countries have includ- ed the shallow hydrate development in their future energy plans, and researchers have initially proposed some min- ing schemes, actual field tests have not yet been conducted.
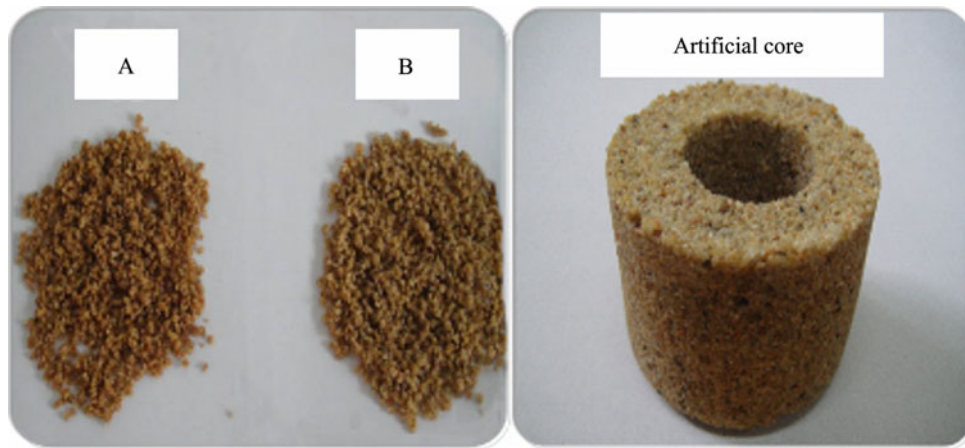
Fig.13 Epoxy resin coated particles and artificial cores.

The fundamental technical problems to be solved are how to avoid the engineering geology risks at shallow depths and improve the bulk hydrate gas production efficiency. In this paper, an alternative design for shallow gas hydrate recovery is proposed, based on the combination of radial drilling, heat injection, and backfilling methods. Its feasibility is assessed by using the reservoir data of the South China Sea. The results show that the soil can provide enough bearing capacity for the conventional well construction at depths of 60 mbsf, and the drilling fluid with densities ranging from 9 to13 ppg can prevent hydraulic fractures. However, with the dissociation of bulk hydrates, the well will face great risks in stability. The suction anchor is recommended as it shows enough load capacity at only 10 mbsf. The numerical simulation results show that, under the constraints of the established model, the average gas production ratio of four branch hole depressurization method is $1720 \, \mathrm{m^3 \, d^{-1}}$. However, with the hot water injection, the average gas production ratio can be increased to about $3500 \, \mathrm{m^3 \, d^{-1}}$. In addition, the backfilling volume in the goaf can be estimated according to the gas production volume. It is possible to realize this scheme with the existing engineering equipment, so it has strong application prospects.

Acknowledgements

References

Aldridge, T., and Haland, G., 1991. Assessment of conductor setting depth. *Offshore Technology Conference*. OnePetro, Texas, OTC-6713-MS.

Allen, J., 1965. A review of the origin and characteristics of recent alluvial sediments. *Sedimentology*, **5** (2): 89-191.

Boswell, R., and Collett, T., 2006. The gas hydrates resource pyramid. *Fire in the Ice*, **6**: 1-4.

Boswell, R., Shipp, C., Reichel, T., Shelander, D., Saeki, T., and Frye, M., *et al.*, 2016. Prospecting for marine gas hydrate resources. *Interpretation*, **4**: SA13-SA24, DOI: 10.1190/INT-2015-0036.1.

Chen, Q., Wu, N. Y., Li, Y. L., Liu, C. L., Sun, J. Y., and Meng, Q. G., 2020. Dissociation kinetics characteristics of nodular methane hydrates and their influence factors. *Natural Gas Industry*, **40** (8): 141-148 (in Chinese with English abstract).

Collett, T., Bahk, J. J., Baker, R., Boswell, R., Divins, D., Frye, M., *et al.*, 2015. Methane hydrates in nature – Current knowledge and challenges. *Journal of Chemical & Engineering Data*, **60** (2): 319-329.

Feng, Y., Chen, L., Suzuki, A., Kogawa, T., Okajima, J., and Komiya, A., 2019. Enhancement of gas production from methane hydrate reservoirs by the combination of hydraulic fracturing and depressurization method. *Energy Conversion and Management*, **184**: 11.

Fujii, T., Suzuki, K., Takayama, T., Tamaki, M., Komatsu, Y. Konno, Y., *et al.*, 2015. Geological setting and characterization of a methane hydrate reservoir distributed at the first offshore production test site on the Daini-Atsumi Knoll in the eastern Nankai Trough, Japan. *Marine and Petroleum Geology*, **66**: 310-322, DOI: 10.1016/j.marpetgeo.2015.02.037.

Kong, L., Zhang, Z. F., Yuan, Q. M., Liang, Q. Y., Shi, Y. H., and Lin, J. Q., 2018. Multi-factor sensitivity analysis on the stability of submarine hydrate-bearing slope. *China Geology*, **1** (3): 367-373, DOI: 10.31035/cg2018051.

Konno, Y., Fujii, T., Sato, A., Akamine, K., Naiki, M., Masuda, Y., *et al.*, 2017. Key findings of the world's first offshore methane hydrate production test off the coast of Japan: Toward future commercial production. *Energy & Fuels*, **31** (3): 2607-2616, DOI: 10.1021/acs.energyfuels.6b03143.

Li, G., Moridis, G. J., Zhang, K., and Li, X. S., 2011. The use of huff and puff method in a single horizontal well in gas production from marine gas hydrate deposits in the Shenhu Area of South China Sea. *Journal of Petroleum Science and Engineering*, **77** (1): 49-68, DOI: 10.1016/j.petrol.2011.02.009.

Li, J. F., Ye, J. L., Qin, X. W., Qiu, H. J., Wu, N. Y., Lu, H., *et al.*, 2018. The first offshore natural gas hydrate production test in South China Sea. *China Geology*, **1**: 5-16.

Li, L., Wang, Y., Xu, Q., Zhao, J., and Li, D., 2012. Seismic geomorphology and main controls of deep-water gravity flow sedimentary process on the slope of the northern South China Sea. *Science China Earth Sciences*, **55** (5): 747-757, DOI: 10.

1007/s11430-012-4396-1.

Li, N., Sun, Z. F., Jia, S., Sun, C. Y., Liu, B., Yang, L.Y., *et al.*, 2019a. A novel method to greatly increase methane hydrate exploitation efficiency *via* forming impermeable overlying CO_2 cap. *Energy Procedia*, **158**: 7.

Li, Y., Wan, Y., Chen, Q., Sun, J., and Wu, N., 2019b. Large borehole with multi-lateral branches: A novel solution for exploitation of clayey silt hydrate. *China Geology*, **3**: 333-341, DOI: 10.31035/cg2018082.

Liu, B., Chen, J., Pinheiro, L. M., Yang, L., Liu, S., Guan, Y., *et al.*, 2021. An insight into shallow gas hydrates in the Dongsha area, South China Sea. *Acta Oceanologica Sinica*, **40** (2): 136-146, DOI: 10.1007/s13131-021-1758-6.

Luan, X., Jin, Y., Obzhirov, A., and Yue, B., 2008. Characteristics of shallow gas hydrate in Okhotsk Sea. *Science in China Series D: Earth Sciences*, **51** (3): 415-421, DOI: 10.1007/s11430-008-0018-3.

Matsumoto, R., and Aoyama, C., 2020. Verifying estimates of the amount of methane carried by a methane plume in the Joetsu Basin, eastern margin of the Sea of Japan. *Journal of Geography (Chigaku Zasshi)*, **129** (1): 141-146, DOI: 10.5026/jgeography.129.141.

Moridis, G. J., 2014. User's manual for the hydrate v1. 5 option of TOUGH+ v1. 5: A code for the simulation of system behavior in hydrate-bearing geologic mediaRep. Lawrence Berkeley National Laboratory (LBNL), Berkeley, CA, United States.

Pape, T., Bahr, A., Klapp, S. A., Abegg, F., and Bohrmann, G., 2011. High-intensity gas seepage causes rafting of shallow gas hydrates in the southeastern Black Sea. *Earth & Planetary Science Letters*, **307** (1-2): 35-46.

Rahim, I., Nomura, S., Mukasa, S., and Toyota, H., 2015. Decomposition of methane hydrate for hydrogen production using microwave and radio frequency in-liquid plasma methods. *Applied Thermal Engineering*, **90**: 120-126, DOI: 10.1016/j.applthermaleng.2015.06.074.

Schicks, J. M., Haeckel, M., Janicki, G., Spangenberg, E., Thaler, J., Giese, R., *et al.*, 2020. Development, test, and evaluation of exploitation technologies for the application of gas production from natural gas hydrate reservoirs and their potential application in the Danube Delta, Black Sea. *Marine and Petroleum Geology*, **120**: 104488, DOI: 10.1016/j.marpetgeo.2020.104488.

Snyder, G. T., Matsumoto, R., Suzuki, Y., Kouduka, M., Kakizaki, Y., Zhang, N., *et al.*, 2020a. Evidence in the Japan Sea of microdolomite mineralization within gas hydrate microbiomes. *Scientific Reports*, **10** (1): 1876, DOI: 10.1038/s41598-020-58723-y.

Snyder, G. T., Sano, Y., Takahata, N., Matsumoto, R., Kakizaki, Y., and Tomaru, H., 2020b. Magmatic fluids play a role in the development of active gas chimneys and massive gas hydrates in the Japan Sea. *Chemical Geology*, **535**: 119462, DOI: 10.1016/j.chemgeo.2020.119462.

Waage, M., Portnov, A., Serov, P., Bünz, S., Waghorn, K. A., Vadakkepuliyambatta, S., *et al.*, 2019. Geological controls on fluid flow and gas hydrate pingo development on the Barents Sea margin. *Geochemistry, Geophysics, Geosystems*, **20** (2): 630-650, DOI: 10.1029/2018gc007930.

Wan, Y., Wu, N., Chen, Q., Li, W., Hu, G., Huang, L., *et al.*, 2022. Coupled thermal-hydrodynamic-mechanical-chemical numerical simulation for gas production from hydrate-bearing sediments based on hybrid finite volume and finite element method. *Computers and Geotechnics*, **145**: 104692.

Wang, L., Zhong, L., Zhou, S., Wang, G., and Fu, Q., 2020. Development of marine natural gas hydrate mining technology and equipment. *Chinese Journal of Engineering Science*, **22** (6): 32, DOI: 10.15302/j-sscae-2020.06.005.

Wu, N. Y., Li, Y. L., Wan, Y. Z., Sun, J. Y., Huang, L., and Mao, P. X., 2020. Prospect of marine natural gas hydrate stimulation theory and technology system. *Natural Gas Industry*, **40** (8): 100-115 (in Chinese with English abstract).

Xu, C. L., Sun, Z. L., Geng, W., Zhang, X. R., Cao, H., Liu, L. P., *et al.*, 2018. Thermal recovery method of submarine gas hydrate based on a thermoelectric generator. *China Geology*, **1** (4): 568-569, DOI: 10.31035/cg2018068.

Yamamoto, K., Wang, X. X., Tamaki, M., and Suzuki, K., 2019. The second offshore production of methane hydrate in the Nankai Trough and gas production behavior from a heterogeneous methane hydrate reservoir. *Royal Society of Chemistry Advances*, **9** (45): 25987-26013, DOI: 10.1039/c9ra00755e.

Ye, J. L., Qin, X. W., Xie, W. W., Lu, H. L., and Ma, B. J., 2020. Main progress of the second gas hydrate trial production in the South China Sea. *Geology in China*, **47** (3): 557-568 (in Chinese with English abstract).

Zhang, X. H., and Lu, X. B., 2016. A new exploitation method for gas hydrate in shallow stratum: Mechanical thermal method. *Chinese Journal of Theoretical and Applied Mechanics*, **48** (5): 1238-1246 (in Chinese with English abstract).

Zhou, S. W., Chen, W., Li, Q. P., Zhou, L. J., and Shi, H. S., 2017a. Research on the solid fluidization well testing and production for shallow non-diagenetic natural gas hydrate in deep water area. *China Offshore Oil and Gas*, **29** (4): 1-8 (in Chinese with English abstract).

Zhou, S. W., Zhao, J. Z., Li, Q. P., Chen, W., Zhou, J. L., Wei, N., *et al.*, 2017b. Optimal design of the engineering parameters for the first global trial production of marine natural gas hydrates through solid fluidization. *Natural Gas Industry*, **37** (9): 1-14 (in Chinese with English abstract).

(Edited by Chen Wenwen)